



# In situ tuning of graphene oxide morphology by electrochemical exfoliation

Pratiksha M. Biranje<sup>1</sup>, Jyoti Prakash<sup>2</sup>, Amit P. Srivastava<sup>2</sup>, Sujoy Biswas<sup>2</sup>, Ashwin W. Patwardhan<sup>2</sup>, Jyeshtharaj B. Joshi<sup>1,3</sup>, and Kinshuk Dasgupta<sup>2,3,\*</sup> 

<sup>1</sup>Department of Chemical Engineering, Institute of Chemical Technology, Mumbai 400019, India

<sup>2</sup>Materials Group, Bhabha Atomic Research Centre, Mumbai 400085, India

<sup>3</sup>Homi Bhabha National Institute, Mumbai 400085, India

**Received:** 10 July 2021

**Accepted:** 13 September 2021

**Published online:**  
27 September 2021

© The Author(s), under exclusive licence to Springer Science+Business Media, LLC, part of Springer Nature 2021

## ABSTRACT

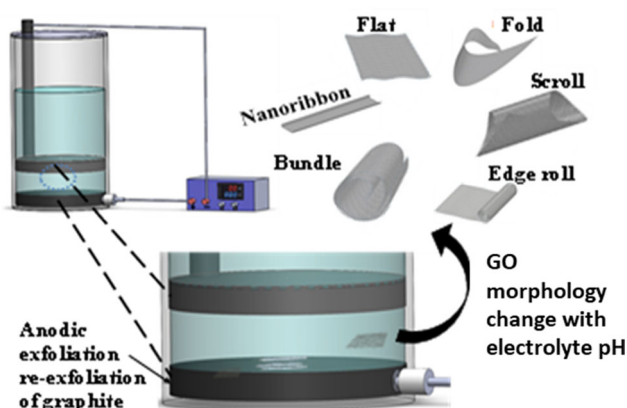
This paper illustrates the electrochemical exfoliation of graphite for the synthesis of graphene oxide (GO) with few layers. Innovative design and arrangement of electrodes were adopted, which allowed simultaneous exfoliation and re-exfoliation of graphite anode. Electrolyte having different molar concentrations of an aqueous solution of sulfuric acid (H<sub>2</sub>SO<sub>4</sub>) and pH offered successful exfoliation of graphite anode with a varying yield of GO. The addition of sodium hydroxide (NaOH) in the solution affected the exfoliation rate and the morphology of the GO sheets. The transition of GO sheets from clumping–scrolling–flat sheet edge rolling to nanoribbons was observed by the change of composition and pH of the electrolyte. GO sheets showed lateral dimensions ranging from 500 nm to 24 μm, and ribbons and scrolls were found to have dimensions up to 50 μm. With the help of transmission electron microscopy, Raman spectroscopy, Fourier transform infrared spectroscopy, X-ray diffraction and X-ray photoelectron spectroscopy, a mechanism of exfoliation has been proposed. In situ functionalization of graphene helped in imparting stability to the GO in solvents such as ethanol and water for more than 11 months. This study elaborates on the significance of solvated sulfate ions and provides a window of sulfate and hydroxyl ion combination for tuning of structural morphologies of GO.

Handling Editor: Annela M. Seddon.

Address correspondence to E-mail: dasguptakinshuk@yahoo.com; kdg@barc.gov.in

<https://doi.org/10.1007/s10853-021-06535-4>

## GRAPHICAL ABSTRACT



## Introduction

Technological development in broad sense roots back to material revolution over the years. The technical evolution has opened a window for research in the development of new materials and their applications. Similarly, the invention of graphene has opened up a window for research in the field of 2-D materials [1].

Graphene is a hexagonal carbon structure having a thickness of a single atomic layer. For practical purposes, graphene with more than one layer may be useful. Graphene properties are attributed to their number of layers, i.e., single layer, few layers (2–10 no of sheets) and multilayer [2]. In the case of a few layers or multilayers, stacked carbon layers are held together with pi bonds. Graphene improves the mechanical strength of the composites by its ability to transfer the load. Likewise, graphene is considered to be a propitious material in the field of electronics [3][3], capacitors [5], sensors [6, 7], energy storage devices [8] due to its high charge transfer capacity and large surface area.

Graphene is a fundamental carbon material, but it needs processing to be obtained in an isolated form. Synthesis routes of graphene involve either depositing hexagonal carbon sheets by pyrolysis of carbon source in the presence of a catalyst (bottom-up approach) or shearing down bulk graphite layers through external forces, developing a carbon array (top-down approach). In the first approach, methods

like chemical vapor deposition [9], arc discharge [10] and in the second approach chemical and mechanical exfoliation routes [11] have been reported. Out of different techniques, liquid-phase chemical exfoliation has the potential for industrial scale-up. In liquid-phase chemical exfoliation, electrolyte ions intercalate in between the graphitic layers to break the pi bonds to generate graphene sheets. Depending on the composition of the electrolyte, these graphene sheets get functionalized with oxygen and form dispersible graphene oxide (GO). The synthesis route always affects the morphology of the GO. Depending upon the domain of functionality, i.e., edge or basal, structural stability of GO is achieved. GO, due to its surface functionality, encounters lesser interfacial tension in the solvent or attraction forces between GO sheets. The nature of the electrolyte solution plays an important role to decide the final morphology and functionality of the resultant product. Functionality can be further reduced with chemical or thermal treatment to restore graphene structure also known as reduced graphene oxide (RGO).

Wet chemical exfoliation approaches using different methods like Staudenmaier [12], Hoffman [13], Hummers [14] and improved Hummers [15] methods yield highly oxidized/distorted graphene structure in resultant GO. Such methods impart structural impairment in the product due to the use of a harsh oxidative environment. The key factors associated with the scalability of the GO/RGO synthesis process

are (1) use of minimal hazardous materials and (2) consistency of electrolyte with the progress of exfoliation [16]. In this view, the report on ultrasonic wave-assisted exfoliation of graphite has an edge over other techniques with ease of operation [17–23]. However, the technique lacks attraction due to high-intensity shockwaves and high local heat generation during the process leading to adversely affected characteristics of the graphene layer [24, 25]. The main drawback of the method is a reduction of lateral dimensions of the graphene lattice.

Further, electrochemical exfoliation of graphite has been successfully employed using various types of mild electrolytes such as anionic, cationic-based ionic liquids, salts, acids and surfactants [26, 27]. In electrochemical exfoliation, there are different routes to apply the bias like, constant DC supply with change of polarity, stepwise increase in the applied potential and continuous DC supply [28]. Liu et al. have reported the synthesis of graphene nanosheets (lateral size  $\sim 500$  nm) using anionic ionic liquids such as 1-octyl-3-methyl-imidazolium chloride ( $[\text{C}_8\text{-mim}]^+\text{Cl}^-$ ) and similar electrolyte with different anions like  $\text{PF}_6^-$ ,  $\text{BF}_4^-$  [28, 29]. The preparation of heteroatom intercalated graphene was also achieved through electrochemical exfoliation [31]. Lu et al. have reported the synthesis of RGO in the form of nanoribbons using 1-methyl-3-butylimidazolium chloride ( $[\text{BMIm}]\text{Cl}$ ) anionic electrolyte [32]. Parvez et al. [33] reported that organic salts anions such as  $\text{ClO}_4^-$ ,  $\text{Cl}^-$  and  $\text{NO}_3^-$  showed no extensive exfoliation. The intercalation and exfoliation could be done sequentially through change of polarity of electrode. This route also enabled the control over graphene thickness [33, 34]. Similarly, though the cathodic exfoliation of graphite has been studied by researchers, this process yielded a low quantity of graphene with poor dispersion stability [30]. Various 2D material like  $\text{MoS}_2$  phosphorous, antimony and bismuth has been widely explored through electrochemical exfoliation method [36, 37].

Similar to planar graphene nanosheets, different morphologies such as nanoscrolls, nanoribbons have also gained attention due to their interesting properties like conductivity, strength, energy storage, etc. [38, 39]. Unlike graphene oxide nanosheets, nanoscrolls and nanoribbons have restricted lateral dimensions due to rolling. Such confined morphologies of graphene oxide offer interesting features because of their synergistic combination of properties

of carbon nanotube (CNT) and graphene. GO nanoscrolls or nanoribbons are one-dimensional structures, and due to their high adhesion strength compared to regular sheet, scrolls are used in strengthening of polymer. Moreover, rolling helps in developing strain in structure that improves its conductivity. Graphene nanoribbon for its unusual conducting properties has found application in biomedicine and sensors [41]. Unzipping CNT by longitudinal cutting, ion intercalation, highly exothermic and oxidative treatment have been attempted successfully to produce graphene nanoribbons within the sub-nanometer range [42]. Figure 1 shows different geometries and nomenclatures of graphene. A list of studies showing the effect of graphite source and electrolyte on GO morphologies is tabulated in Table 1.

Until now, in the top-down approach, the researchers focused on generating GO/RGO using different electrolytes in conventional vertical two-electrode cell assemblies, where random exfoliation of graphite occurs with applied bias potential that leads to the formation of random-sized GO/RGO particles. Then, different sized graphene particles are segregated using the centrifugation method, but the yield of uniform size graphene particles always remains low. So the real problem for mass-scale production of GO/RGO primarily depends on the electrode cell assembly design followed by the type of electrolyte.

Herein, we report a simple strategy for the synthesis of GO scrolls, sheets and ribbons. For the first time, self-rolling of sheets is studied by tuning the electrolyte composition. This method avoids the additional step of pH adjustment after GO synthesis to achieve various morphologies of GO as during the exfoliation process only we can achieve it. An innovative cell design has been employed for GO synthesis using an electrochemical exfoliation approach. All the experiments were carried out at constant current conditions. It was observed that the exfoliation under the constant current approach has the edge over the exfoliation under the constant voltage condition, regardless of the electrolyte composition. With the consideration of the intercalation properties of sulfate ions, aqueous sulfuric acid was used as the electrolyte. The effect of neutralized acid on exfoliation and morphology was studied by the addition of NaOH to the aqueous  $\text{H}_2\text{SO}_4$  solution. This approach allows a narrow size distribution of GO

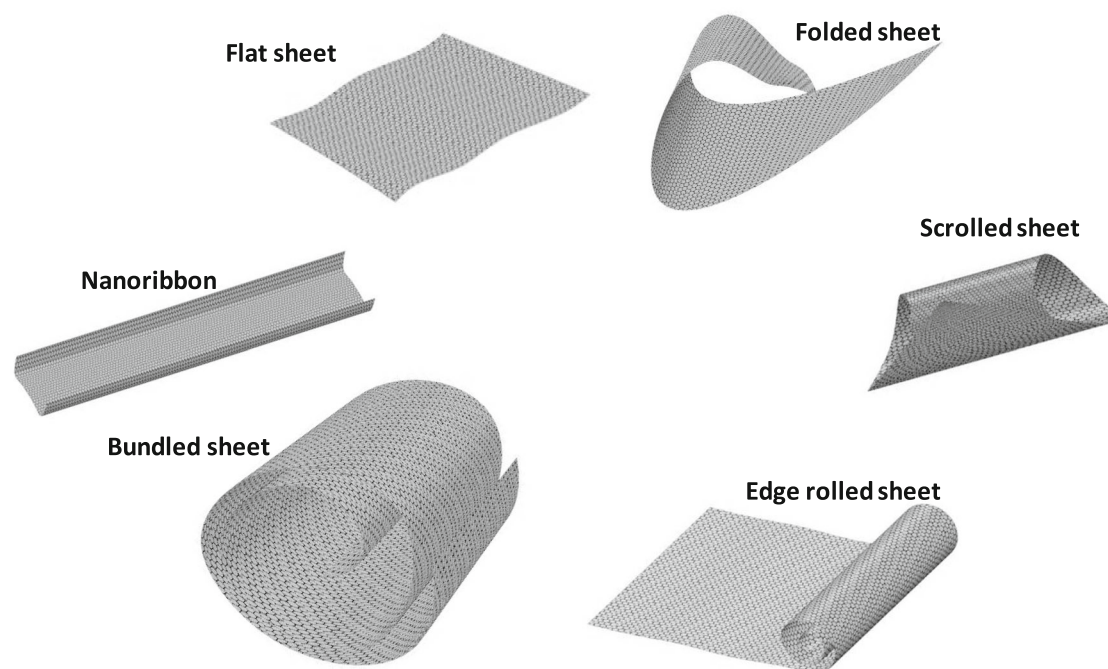


**Figure 1** Different geometries of graphene sheets.

morphologies through multiple exfoliation and re-exfoliation of anodic graphite. Detailed characterizations of the GO were carried out using UV spectrometry, Raman spectroscopy, TEM, XRD, FTIR and XPS.

## Experimental

### Materials

A graphite block (density 1.84 g/cc) was procured from M/s Amit Engineers, Mumbai, India, and was machined into round disks (80 mm diameter, 10 mm thick) and used as the anode and the cathode. Sulfuric acid ( $\text{H}_2\text{SO}_4$  98%, AR) and sodium hydroxide (NaOH pellets AR) were purchased from SD Fine-Chem Limited, India. Deionized water was used from the in-house plant. Polyvinylidene difluoride (PVDF) membrane of pore size 0.22  $\mu\text{m}$ , diameter 47 mm and thickness 125  $\mu\text{m}$  was purchased from MERCK. All chemicals were used as received, without further purification.

### Methods

Figure 2 shows the schematic of the experimental setup. A glass vessel having one small side opening was used. Two graphite disks with similar

dimensions were taken as the anode and the cathode. Anode was provided with a small hole on the thickness side, and the cathode was screwed from the top surface for inserting a connecting graphite rod into it. The connecting rod of the cathode was held in position with the help of a polypropylene lid having a rod size opening in it. The cathode rod could be moved vertically to adjust the distance between two graphite electrodes. These contacting graphite rods were clamped with stainless steel conducting clips to provide current from a DC supplier. A horizontal parallel arrangement of graphite electrodes, where maximum areas of the electrodes were facing each other, was used to achieve the advantage of the re-exfoliation process. Due to the horizontal arrangement, if any large particle exfoliates from the anode, it is expected to fall on the same anode surface. In this way, the contact is maintained between incompletely exfoliated graphite chunks and the anode. A completely exfoliated graphene enters into the supernatant. This method helps in improving the yield of the process as well as the reduction of the number of layers.

For electrochemical exfoliation of graphite, 500 ml solution of (1) aqueous sulfuric acid and (2) a mixture of sulfuric acid and sodium hydroxide was used as the electrolytes. The DC supply was started and the

**Table 1** List of studies showing the effect of graphite source and electrolyte on GO morphology synthesized by a top-down approach

Sr. no	Graphite source	Method	Electrolyte/exfoliation medium	Lateral dimensions	Ref
1	Pre-exfoliated graphite (HM)	Multiple sonication	Water (60 °C)	(Monolayer) $\approx 1 \mu\text{m}$ to $\approx 950 \text{ nm}$	[17]
2	Graphite (1200, 300–500, > 80 mesh)	Modified Hummers	(23 mL) $\text{H}_2\text{SO}_4$ + (3 g) $\text{KMnO}_4$ + HCl (30 mL) $\text{H}_2\text{SO}_4$ + (3 g) $\text{KMnO}_4$ + HCl (60 mL) $\text{H}_2\text{SO}_4$ + (3 g) $\text{KMnO}_4$ + HCl	(Monolayers > 90%) $1.7 \pm 1.0$ , $14.9 \pm 8.3$ , $38.0 \pm 16.3 \mu\text{m}$	[18]
3	Graphite powder (325 mesh)	Sonochemical (Hummers method + Ultrasonic)	$\text{NaNO}_3$ + $\text{H}_2\text{SO}_4$ + $\text{KMnO}_4$	(Creased mono- to few-layered planar sheet) > 200 nm	[19]
4	Graphite powder (325 mesh)	Sonochemical (Improved Hummer + Ultrasonic)	$\text{H}_3\text{PO}_4$ + $\text{H}_2\text{SO}_4$ + $\text{KMnO}_4$ + HCl + $\text{H}_2\text{O}_2$	(Folded FLG) > 100 nm	[23]
5	Natural graphite (La82.8, Lc59.5 nm) Synthetic graphite (La65.4, Lc26.2 nm)	Modified Hummers + Ultrasonic	$\text{NaNO}_3$ + $\text{H}_2\text{SO}_4$ + $\text{KMnO}_4$ + $\text{H}_2\text{O}_2$	(mono- and few-layered planar sheet) $\approx 1.5$ , $\approx 0.75 \mu\text{m}$	[24]
6	Graphite powder (200 $\mu\text{m}$ )	Modified Hummers	$\text{NaNO}_3$ + $\text{H}_2\text{SO}_4$ + $\text{KMnO}_4$ + $\text{H}_2\text{O}_2$	500 $\mu\text{m}^2$	[25]
7	HOPG (1 cm:1 cm:1 mm)	ECE	1-methyl-3-butylimidazolium tetrafluoroborate + Water	Carbon nanocrystal 8–10 nm, nanoribbons $10 \times (60 \pm 20) \text{ nm}$ , ultrathin graphene sheet 200–500 nm	[29]
8	Graphite rod (6 mm dia.)	ECE	Deep eutectic solvent + Ionic liquid + Acetonitrile	FLG > 5 $\mu\text{m}$	[30]
9	Graphite rod	ECE	1-octyl-3-methyl-imidazolium hexafluorophosphate, 1-octyl-3-methyl-imidazolium tetrafluoroborate, 1-octyl-3-methyl-imidazolium chloride, 1-butyl-3-methyl-imidazolium hexafluorophosphate	Crumpled sheets 700 nm	[32]
10	Graphite flake	ECE	$(\text{NH}_4)_2\text{SO}_4$ , $\text{Na}_2\text{SO}_4$ , $\text{K}_2\text{SO}_4$	FLG 5–44 $\mu\text{m}$	[33]
11	HOPG (3.0 $\times$ 0.5 $\text{cm}^2$ )	ECE	0.1 M $\text{H}_2\text{SO}_4$	FLG 3 $\mu\text{m}$	[43]
12	Graphite flake (325 mesh)	Chemical exfoliation	123.6 g Urea/300 mL Glycerin/0.2 g Sodium hydroxide	FLG 6–8 $\mu\text{m}$	[44]
13	Graphite rod	ECE	0.1 M $(\text{NH}_4)_2\text{SO}_4$	FLG 5.0–3 $\mu\text{m}$	[45]
14	Natural graphite flakes (99.8%)	Modified Hummer	GO/ $\text{MnO}_2$ / $\text{H}_2\text{O}_2$ (30%)	Nanoscroll > 0.2 $\mu\text{m}$	[46]
15	Natural graphite flake (32–325 mesh)	Modified Hummers	GO/liq. nitrogen	$\sim 10 \mu\text{m}$ Nanoscroll	[47]
16	Natural graphite flake (500–600 $\mu\text{m}$ )	Modified chemical exfoliation	$\text{NaNO}_3$ + $\text{H}_2\text{SO}_4$ + $\text{KMnO}_4$ + $\text{H}_2\text{O}_2$ (30%)	FLG 10–300 $\mu\text{m}$	[48]
17	Graphene	Bubble-induced scrolling	$\text{NaHCO}_3$	Nanoscrolls	[49]
18	MWCNT	Micro-explosion	K/Ar	Nanoribbon 0.5 to 5 $\mu\text{m}$	[42]

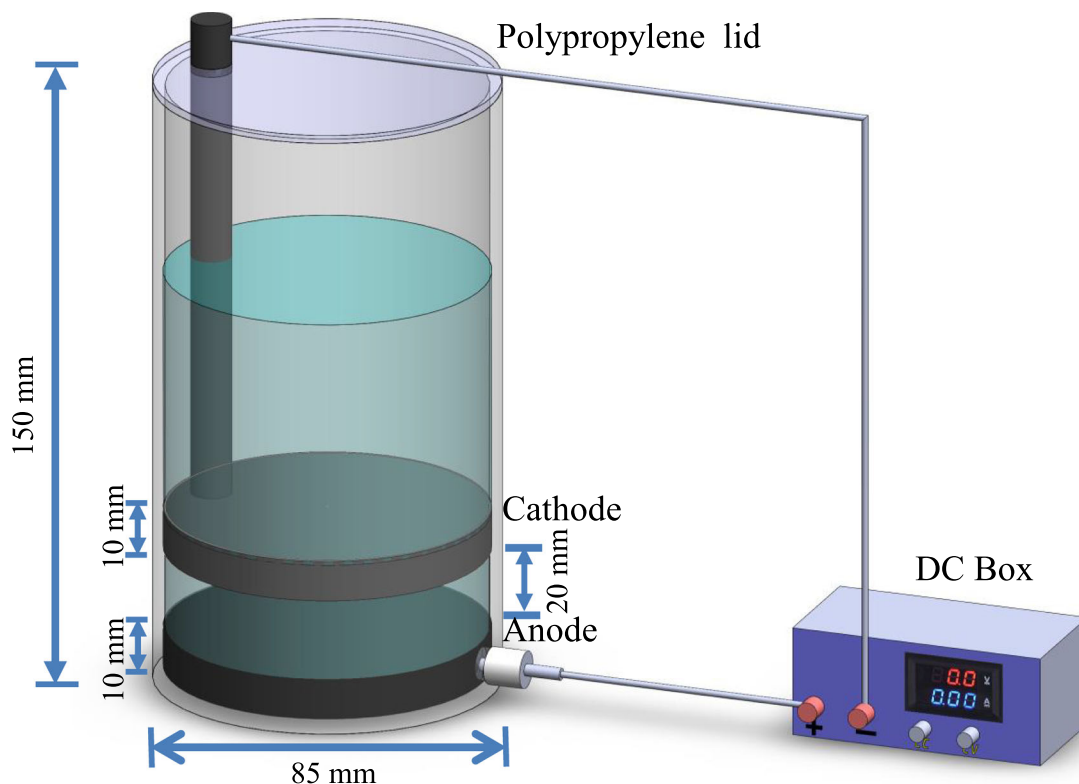


**Figure 2** Schematic diagram of the experimental setup used for the electrochemical exfoliation.

**Table 2** Electrolyte concentration used for samples during electrochemical exfoliation

Electrolyte	Sample	pH	Sulfuric acid (M)	NaOH (M)	Rate ( $\text{mg}/\text{cm}^2 \times \text{s}$ )
$\text{H}_2\text{SO}_4$	GO1	0.32	0.4	–	$6.48 \times 10^{-05}$
	GO2	0.2	0.5	–	$1.68 \times 10^{-04}$
	GO3	0.1	0.6	–	$1.80 \times 10^{-04}$
Constant $\text{H}_2\text{SO}_4$ ( $\text{H}_2\text{SO}_4 + \text{NaOH}$ )	GO4	1.0	0.5	0.75	$2.93 \times 10^{-04}$
	GO5	1.5		0.85	$1.74 \times 10^{-04}$
	GO6	3.6		0.95	$5.85 \times 10^{-05}$
	GO7	8.2		1	$8.35 \times 10^{-05}$
	GO8	11.2		1.1	$1.30 \times 10^{-04}$
Constant pH ( $\text{H}_2\text{SO}_4 + \text{NaOH}$ )	GO9	2.5	0.4	0.85	$6.48 \times 10^{-05}$
	GO10		0.5	0.95	$2.21 \times 10^{-04}$
	GO11		0.6	1	$1.75 \times 10^{-04}$
	GO12		0.7	1.2	$1.84 \times 10^{-04}$

current was maintained at 2A (corresponding current density:  $40 \text{ mA}/\text{cm}^2$ ) with a 6 V supply throughout the experiment. The system took a few minutes to get stabilized once the bias was applied.

Experiments were carried out as shown in Table 2 at room temperature conditions. After each experiment, the resultant liquid was kept idle for 16 h to separate/settle the large chunks of graphite from

mother liquor because of their weight. Exfoliated GO formed a stable dispersion in an electrolyte; therefore, separation of settled larger chunks became easy. The concentration of GO in the solution was measured by a UV spectrometer, and the data were used to get the estimation of the mass of GO exfoliated. After that, the electrolyte was filtered using a vacuum-assisted membrane filtration unit. The final product collected

on the membrane surface was washed three times to make it free from electrolyte residue. Then the purified GO was dispersed in ethanol with the help of sonication. This dispersion was used to make samples for further characterization.

Structural details of graphene oxide samples were studied by transmission electron microscopy (TEM), JEM2100 (JEOL) with an accelerating voltage of 200 kV. X-ray photoelectron spectroscopy was used and XPS spectra were recorded using AXIS Supra (Kratos Analytical, UK) with pressure maintained  $< 2.0 \times 10^{-7}$  Pa in the instrument. XPS analysis was carried out with an X-ray excitation source monochromatic Al ( $K\alpha$  75 W) with a takeoff angle of  $90^\circ$ . To obtain specific elemental quantification of carbon and oxygen, high-resolution scans pass energy  $E_p = 20$  eV (resolution  $\sim 0.5$  eV) were used. A survey scan was carried out at 160 eV (resolution  $\sim 2$  eV). Raman spectra were recorded to determine the characteristic of graphene oxide using WITec alpha-300R, GmbH with laser wavelength 514 nm for all the samples. Laser intensity was chosen carefully to avoid sample burning or damage. Powder X-ray diffraction (XRD) measurement was taken using a tabletop XRD instrument (Proto Make, Canada) with Cu  $K\alpha$  ( $\lambda = 1.5405 \text{ \AA}$ ) as the monochromatic X-ray source in the scanning range ( $2\theta$ ) of  $9\text{--}60^\circ$  and step size of  $2^\circ/\text{min}$ . Fourier transform infrared (FTIR) spectra were acquired using a Bruker TENSOR27 instrument, under room temperature and atmospheric pressure.

## Results

### Electrochemical exfoliation

To evaluate the exfoliation rate of the graphene oxide, the electrolyte sample was collected periodically from the reaction volume. An absorbance at 660 nm vs. concentration graph was plotted for GO solution with known concentrations using a UV spectrometer. From the graph, the unknown concentrations of GO in the electrolyte were determined. The details can be found in the supplementary information (SI). As a result of hydroxyl ion and solvated sulfate ion intercalation, a successive expansion and exfoliation was observed at the anode. In the beginning, as the rate of exfoliation was lower, no color change in the solution was observed. As time passed, increasing

concentration of graphene oxide turned the electrolyte color from colorless to pale yellow and then finally dark brown. Table 2 summarizes the list of experiments and corresponding observations. Figure 3a and b shows the changes in the color of the solution as well as the absorbance in the UV spectra of sample GO3 and GO11 (Refer Table 2), respectively, with time. As per our observation, the initial 2-min period can be denoted as the induction period, where energy is consumed for electrolyte ionization and wetting of graphite. With the increased time of exfoliation, the absorbance increases, and the color darkens. As given in Table 2, three different sets of experiments were carried out, which are explained in the following sections.

### Effect of electrolyte concentration

The electrochemical exfoliation of graphite was studied at different electrolyte concentrations. While studying the effect of increased sulfuric acid concentration, we restricted the study up to 0.6 M (aq.  $\text{H}_2\text{SO}_4$ ) concentration considering the lower limit of the pH scale. On the other side, lowering the molarity also affected GO production. Initially, acid concentration was increased from 0.4 M to 0.6 M as shown in Table 2 for samples GO1–GO3 to observe its effect on graphene oxide. After exfoliating for 6 h, the weight of GO in the electrolyte was measured from UV absorbance data. It was observed that as the concentration of electrolyte increased and the composition of electrolyte changed, the resultant GO exfoliation rate also varied. The rate of graphene oxide exfoliation increased from GO1 to GO3 with an increase in sulfuric acid concentration from 0.4 M to 0.6 M. The increase in the exfoliation rate for these sets of samples GO1 to GO3 is due to the enhanced intercalation of anions with an increase in sulfuric acid concentration.

### Effect of increasing electrolyte pH at constant sulfuric acid concentration

The effect of increasing pH of electrolyte solution on the GO properties and its synthesis rate was studied at a constant sulfuric acid concentration as mentioned in Table 2 (sample GO4 to GO8). For this particular set of experiments, the sulfuric acid concentration was kept constant at 0.5 M, and then, the solution was neutralized with NaOH to increase the pH of the

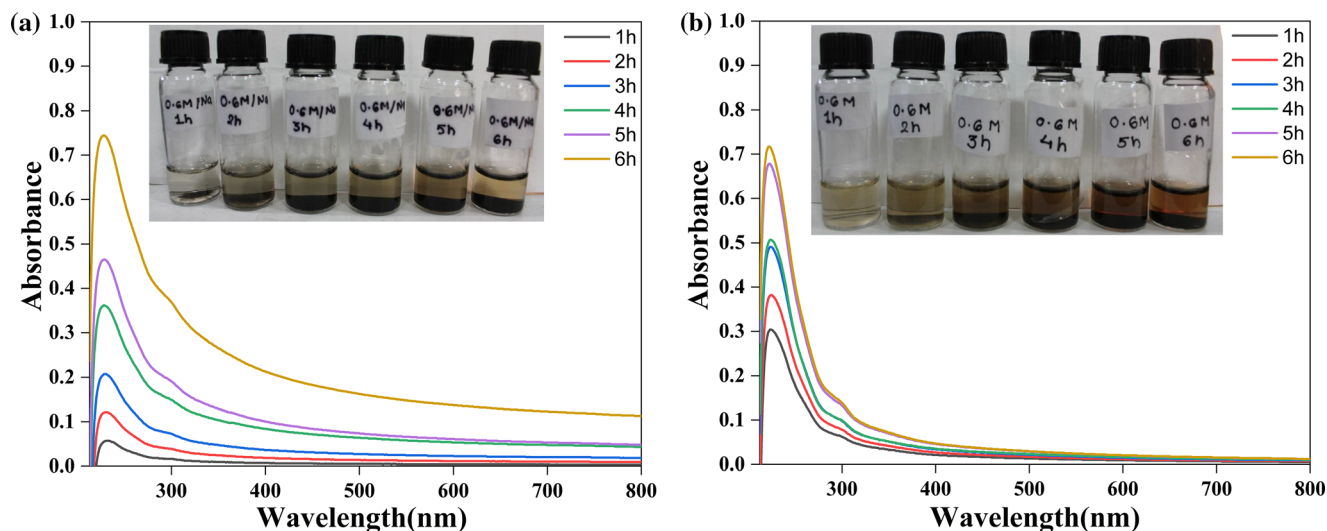


**Figure 3** Changes in absorbance of UV spectra and color of the GO solution (inset) for samples **a** GO3 and **b** GO11.

electrolyte solution. The effect of NaOH addition can be divided into two regions, namely acidic and basic regions. It was observed that the exfoliation rate was high initially in the acidic range and then slowed down. This behavior could be attributed to the hindrance created by the excess sodium ions on the solvated sulfate ion mobility in the electrolyte in the acidic region, thus reducing the intercalation rate. Then the exfoliation rate again slightly increased in the basic region (e.g., sample GO8), which might be due to excessive hydroxyl ion concentration that are coming from addition of NaOH and helped in boundary functionalization and thus caused an increase in exfoliation. As the hydroxyl ions have higher mobility, they reach the graphite anode and oxidize it after bias application. In this study, the increase in pH led to the formation of thicker GO particles. From the recovery (collected GO mass after filtration) point of view, the sample GO4 showed the highest performance.

### Effect of sulfuric acid concentration at constant pH

In this study, the pH of the electrolyte was kept constant with the help of NaOH addition. However, the sulfuric acid concentration increased from 0.4 M to 0.7 M as shown in Table 2 for samples GO9–GO12. The exfoliation was studied at 25 °C maintaining a constant current. It was observed that despite constant pH conditions, the exfoliation rate increased as the sulfuric acid concentration increased (up to G10).

After a certain value of sulfuric acid concentration, the large graphite particles started exfoliating, and hence, the rate of exfoliation of GO could not improve further. Maybe from sample G11 onwards, the excess  $\text{Na}^+$  ions hindered the movement of sulfuric acid; thus, the effectiveness of intercalation got reduced.

### Dispersion stability of GO

All the samples of GO, obtained from different exfoliation conditions, were dispersed into ethanol and water. A stable dispersion of GO was observed in both solvents. The dispersion stability was studied over 11 months. There was no settling of GO observed. Figure 4 depicts the dispersion stability of the GO samples (GO2, GO4 and GO10) with concentration 1 mg/ml over 11 months as analyzed by UV absorbance and also visually. To form stable dispersion, the surface energy of the solvent should match with that of the GO. The formation of stable dispersion in a polar solvent is due to the presence of oxygen functionality on the graphene structure. Due to functionalization, there is an improved interaction between graphene oxide and polar solvents.

### Compositional and structural characterization

#### *X-ray photoelectron spectroscopy (XPS)*

Elemental quantification was carried out using XPS (wide scans and high-resolution scans for C1s and O1s) for different GO samples. Surface



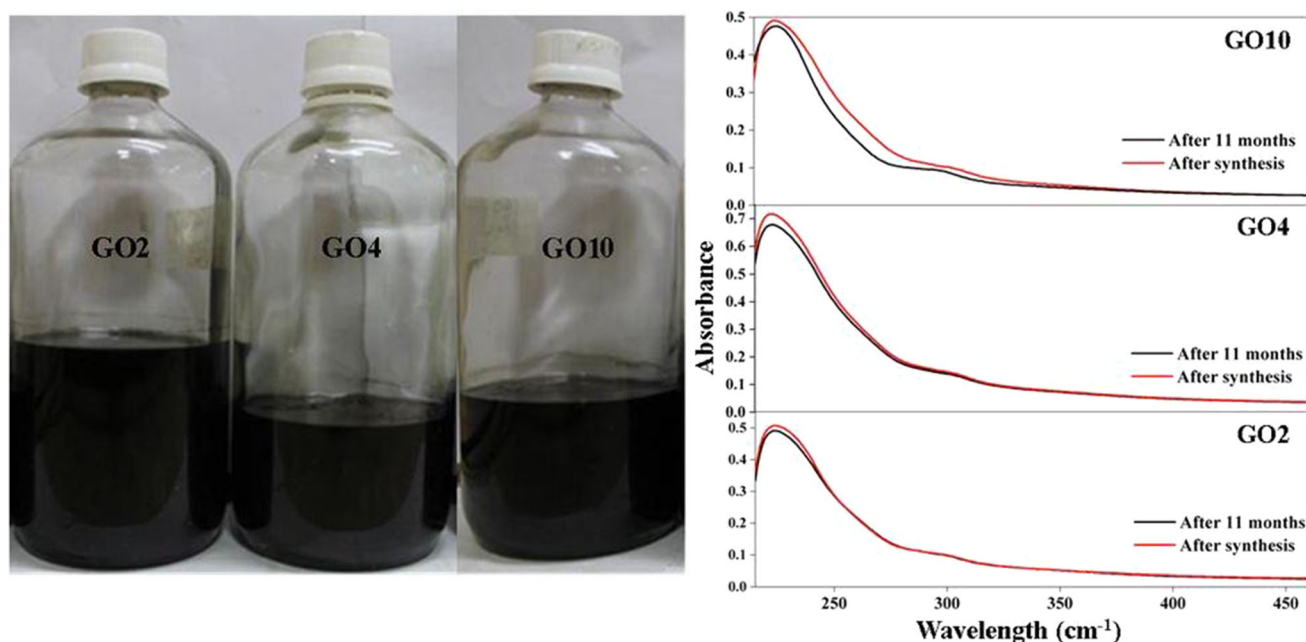


**Figure 4** Representative images ethanol-GO dispersion stability over 11 months for sample, GO2, GO4 and GO10 and their UV absorbance measured after 11 months for comparison.

functionalization of carbon structure with hydroxyl, carboxyl and carbonyl groups was identified by deconvoluting the C1s and O1s spectra by Lorentzian-Gaussian mix function.

C1s signal of GO consists of several functional groups, which can be deconvoluted to find the respective atomic percentage of groups, such as carbon-carbon bonds C=C (284.5 eV) and C atoms bonded to hydroxyl group C-OH, epoxide C-O-C (286.5 eV), carbonyl C=O (287.6 eV) and carboxyl groups -COOH (289.1 eV)[50]. However, there may be slight shift in the values depending on processing conditions. The binding energy data of deconvoluted

C1s and O1s peak obtained for individual GO sample are shown in Table S1 in supplementary information. Figure 5 shows the C1s plots for the representative samples GO2, GO4 and GO10 considering their different synthesis conditions. After oxidation, the C-C area percentage decreased. As per peak deconvolution, all of these samples possess oxidation on basal planes as well as edges. But according to area percentage analysis, the amount of loading of the group like epoxy was increased with respect to pH. With maximum C-C retention, the carboxyl group was absent in sample GO2, where the rest other samples

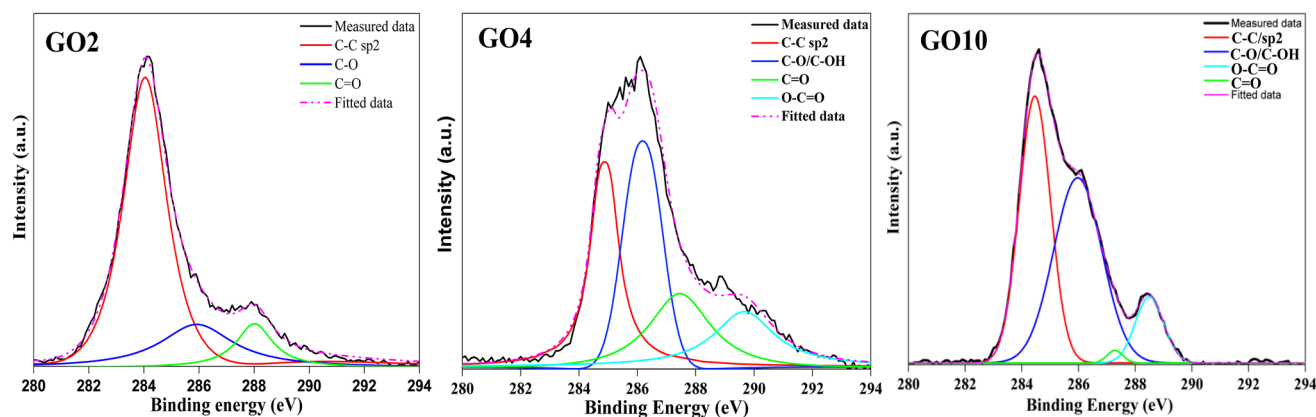


**Figure 5** C1s peaks deconvoluted to analyze oxygenated carbon groups present in respective GO samples.

were seen to possess shown in Fig. S1 in Supporting Information.

The graph in Fig. 6 shows the percentage of carbon functional groups estimated from C1s peak deconvolution. The carbon to oxygen atomic percentage ratio is also plotted. It can be seen from the C/O ratio plot, as the sulfuric acid concentration increases, the resultant oxygen groups on the GO sample increase. Even at constant pH conditions, similar results were observed. Sample in increasing pH conditions showed a gradual drop in oxygen loading capacity from sample GO4. This might be due to the effect of increased OH groups, taking part in engaging grain boundaries during functionalization and exfoliation while retarding the sulfuric acid to interact with the graphite surface through electrostatic repulsion. From XPS, it was observed that there was increase in carbon percentage with increase in the electrolyte pH. This indicates that the total functional group that were necessary to stabilize the graphene sheet decreased with increased pH (basic). This could be

due to the deprotonation of carboxyl groups on graphene. It caused destabilization of sheets resulting in rolling up or folding to minimize the energy. Similar observations were reported by Wu et al. [51] while studying electrochemical activity of graphene oxide in alkaline and acidic pH environment.

Similarly, O1s consists of different functional group peaks merged to give a single large O1s signal. The functional group peaks are C-O (530.5 eV), C-OH (531.4 eV), C=O (535.4), O=C-O (535.4 eV) and -C-O-C (533.4 eV) [52–58]. Figure 7 depicts the deconvoluted O1s spectra for three representative samples deconvoluted into three peaks. The more oxygen percentage on basal plane groups like quinone was observed for GO2 at 530.6 eV. GO4 was rich in oxygen signal bonded to carbon structure at 533.4 eV and carboxyl group at 534.8 eV. With the increasing oxidation, the edge groups like carbonyl, epoxy or carboxyl were seen appearing on GO sheets. It is seen from the graph that both the data (C1s and O1s) are in good agreement with each other. Figure S2 of the

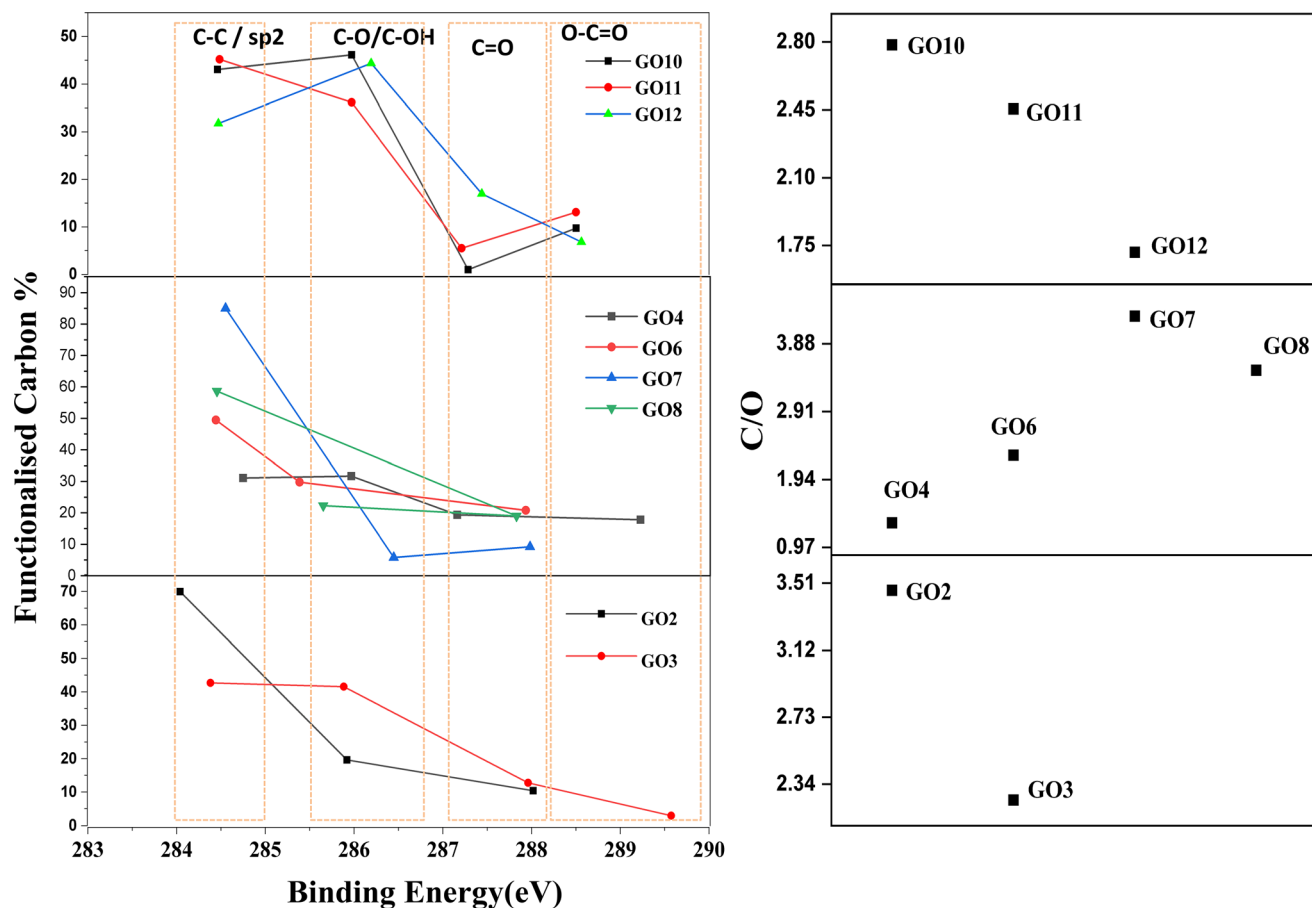


**Figure 6** Functional group percentage and C/O ratio for different GO samples based on C1s peak area analysis.

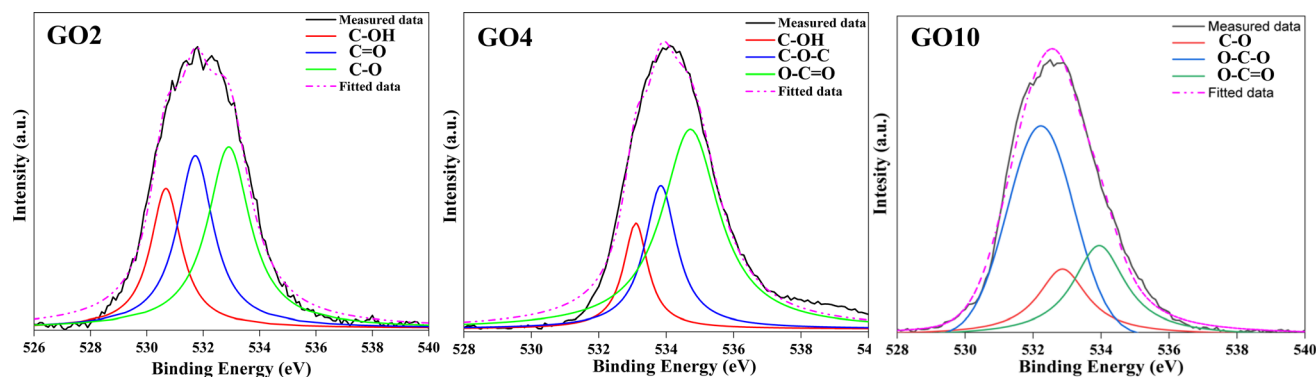


**Figure 7** O1s peaks deconvoluted to analyze oxygenated carbon groups present in representative GO samples.

Supplementary Information contains the information regarding O1s of the rest of the samples.

A structural modification of the carbon array from  $sp^2$  to  $sp^3$  was seen as an effect of increased oxidation. As oxygen percentage increased, the resultant C/O ratio decreased. Similarly, sample GO4 exfoliated with moderate rate and gave fine nanosheets possessed the highest oxygen loading. Although the samples were synthesized after partial neutralization, their effect on reducing oxidation degree is not seen. This scenario might be due to the availability of extra OH groups from NaOH. The highest oxidation was seen in sample GO4. Figure 6 brings out the clarity about the changes in functional groups with respect to electrolyte pH and also the C/O ratio. The samples synthesized at constant pH conditions have shown increasing oxidation degree with respect to an increase in the sulfuric acid concentration. This shows the dependency of oxidation upon oxidizing agent concentration.

### Transmission electron microscopy (TEM)

TEM images of the GO samples are shown in Figs. 8 and 9. GO samples synthesized with only  $H_2SO_4$  electrolyte (GO1 to GO3) are shown in Fig. 8 with corresponding high-resolution TEM (HRTEM) images as a, b and c. Sometimes, a part of the graphene sheet rested on another sheet while drying or rolled into a scroll. These overlapped regions are visibly darker compared to the individual ones. The rolling and folding of sheets at edges were observed and that was due to minimization of surface area. In sample GO1 and GO2, rolling and agglomeration of sheets were observed, whereas, in sample GO3, sheets were folded. Information obtained from TEM images

reveals that samples GO1 and GO2 have 4–15 number layers with a lateral dimension of 500 nm–3  $\mu$ m. Sample GO3 has fewer graphene layers with a longer lateral dimension. These sheets were not clumped; rather, they were folded. If the XPS result is referred, the oxygen functionality increases from GO1 to GO3. Due to very little oxygen functionality, GO1 is rolled, whereas GO3 is just folded as more oxygen functionality has prevented it from rolling.

Figure 9 shows the images of the GO samples obtained with NaOH addition (GO4–GO8) at constant sulfuric acid concentration. The corresponding HRTEM images are shown as (a–e). Sample GO5 shows scrolled nanosheets, whereas sample GO6 depicts bundled sheets. Samples GO7 and GO8 are fibrous, where the fiber length is few microns. The HRTEM images reveal that these are very high-aspect-ratio GO sheets. The basic pH range might have played some role in the formation of the fibrous structure, which is still not well understood.

### Raman spectroscopy

In the Raman spectra typical G ( $1580\text{--}1620\text{ cm}^{-1}$ ), D ( $1342\text{--}1358\text{ cm}^{-1}$ ) and 2D ( $2640\text{--}3180\text{ cm}^{-1}$ ) peaks are seen (Figs. 10, 11 and 13). Figure 10a depicts the change in ID/IG ratio for samples GO1 to GO3; Fig. 10 (b) shows the shift in G peak position and values of FWHM for these samples. An increase in the value of FWHM and a shift of G peak toward a higher value indicate an increase in disorderliness in the structure of GO [57–62]. The trend for sample GO1 to GO3 is in agreement with the earlier discussions which brought out the fact that more oxygen functionalization in GO3 led to more disorderliness. Similarly, the trend is explained for samples GO4 to

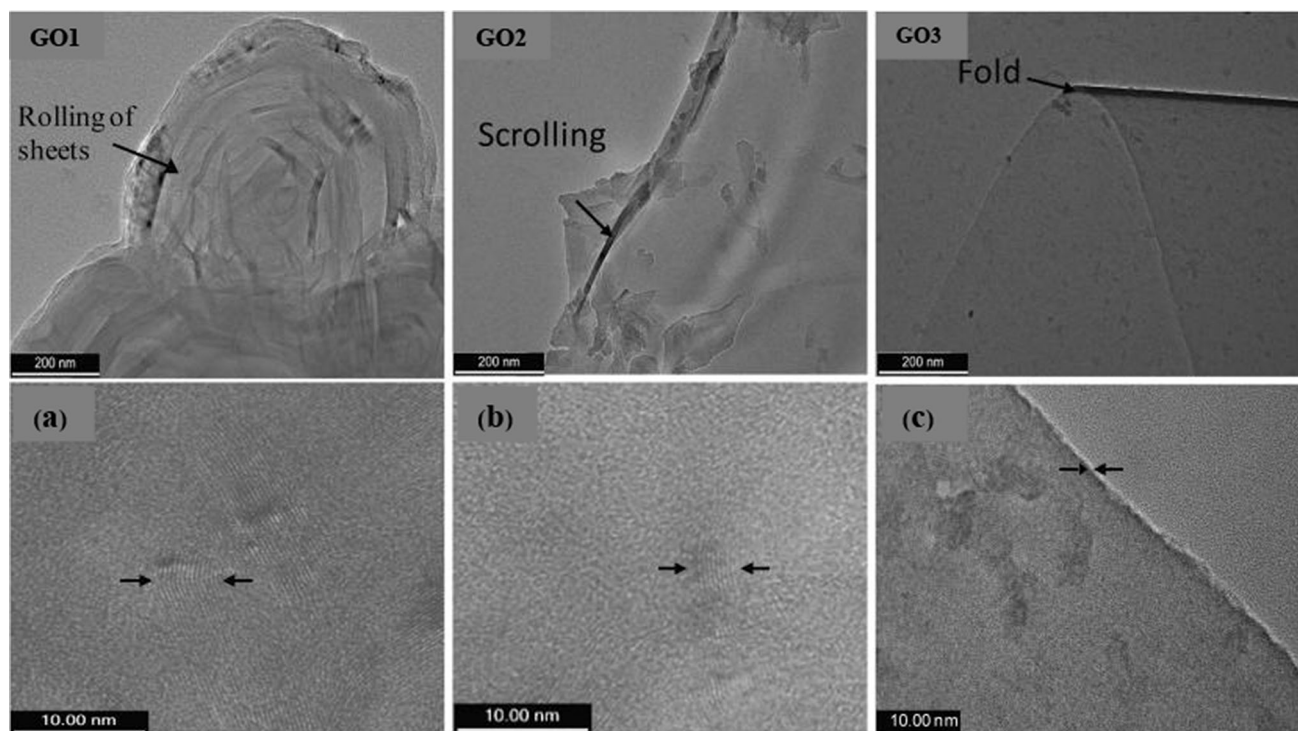


**Figure 8** TEM images of graphene oxide sheets of sample GO1, GO2 and GO3 and their respective HR-TEM images shown as **a**, **b** and **c**.

GO8 in Fig. 11a, b and for samples GO9 to GO12 in Fig. 12a, b. As Fig. 11 b shows, the G band position shifted to lower position upon scrolling up of graphene sheet. Similar observations were reported by Li et al. [65]. These results are compatible with XPS and TEM results shown earlier. During the intercalation and deintercalation process, graphite structure expansion and defect generation via replacement of double-bonded carbon or attachment of oxygen take place. It is to be noted that, during continuous exfoliation and re-exfoliation of graphite, a different percentage of oxygen loading along with structural change happens in the structure. The phenomenon of peak shifting has been explained according to defect density variation with the help of deconvolution of D, G and 2D peaks in Fig. 13 [59].

Figure 13a, b shows the deconvoluted D, G and 2D peaks for sample GO4. The high intensity of the D peak suggests disturbances in  $sp^2$  hybridization due to functionalization. The presence of defects causes the splitting of these peaks. The deconvolution of these peaks with Gaussian fit helps to analyze defects present in the few-layered graphene.  $D^*$  ( $1250\text{ cm}^{-1}$ ) and  $D^{**}$  ( $1500\text{ cm}^{-1}$ ) can be attributed to substitution/disappearance of  $sp^2$  region with heteroatoms

and C-H vibration or defect increment.  $D'$  band causes G band shifting and broadening toward  $1610\text{ cm}^{-1}$  as a result of defective sites, present in the few-layered graphene. Similarly, Fig. 13b shows the deconvoluted 2D peak. The hump of 2D consisted of four peaks  $G^*$  ( $\sim 2400\text{ cm}^{-1}$ ),  $G'$  ( $\sim 2700\text{ cm}^{-1}$ ),  $D + D'$  ( $2930\text{ cm}^{-1}$ ) and  $2D'(G + D')$ , indicating defective few-layered graphene. Because of disturbed planar structure, the 2D peak is always has broadened spectra [59].

#### *X-ray diffraction*

XRD patterns of samples GO1, GO4 and GO9 are given in Fig. 14a, b and c. The characteristic (001) peaks at  $11.37^\circ$ ,  $10.9^\circ$  and  $11.03^\circ$  of sample GO1, GO4 and GO9 confirm the formation of GO with d-spacing 0.77, 0.81 and 0.80 nm, respectively, calculated using the Bragg's law.

#### *Fourier transform infrared spectroscopy*

FTIR helps in analyzing the functional groups present on GO. Different prominent peaks were detected (see Fig. 15) in the GO samples, such as C–O

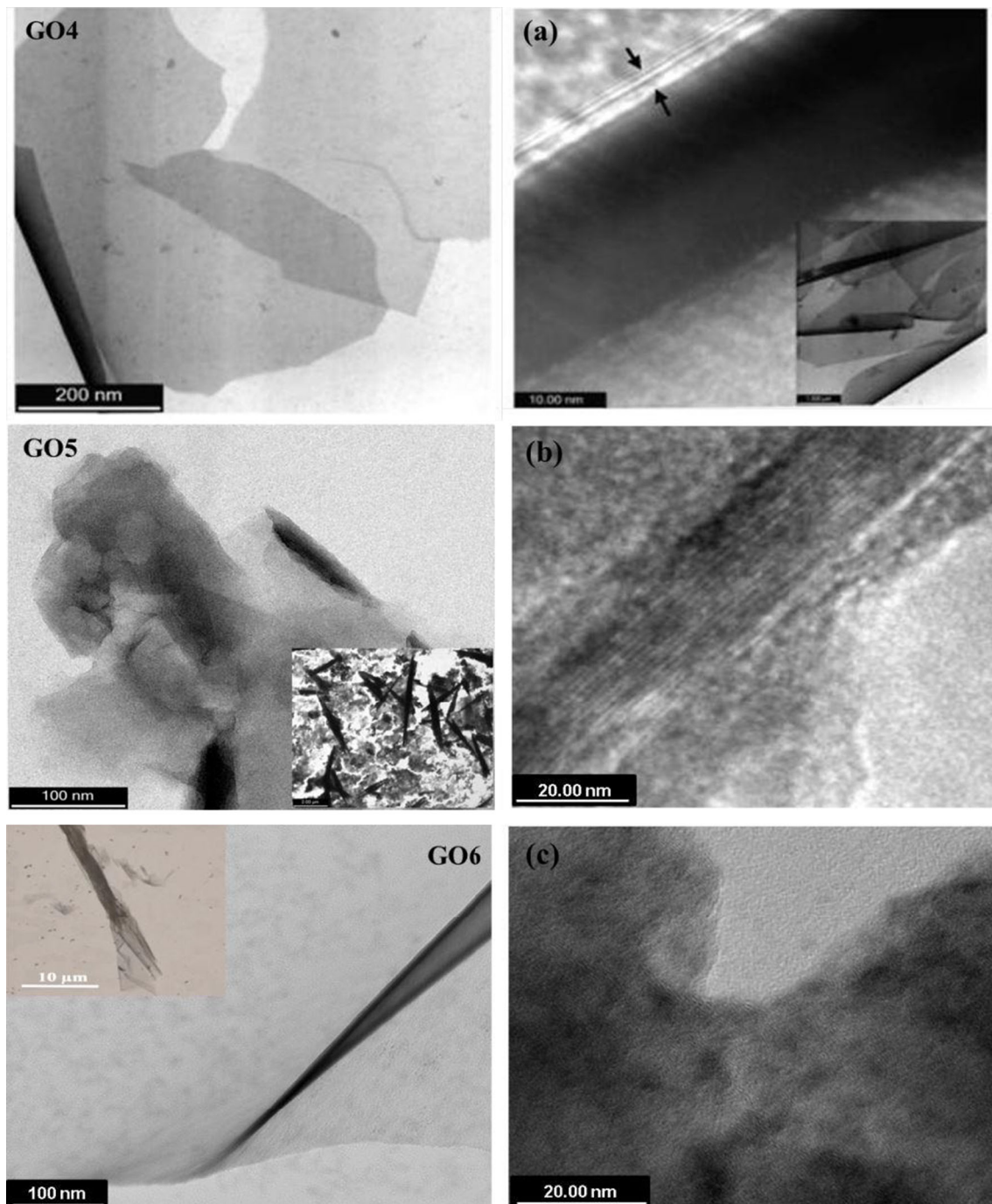


**Figure 9** TEM images of GO sample obtained at different pH conditions for sample GO4, GO5, GO6, GO7 and GO8, and their HR-TEM images shown in a, b, c, d and e, respectively.

vibrations at  $1040\text{--}1080\text{ cm}^{-1}$ , epoxy group (C–O–C) at  $1200\text{--}1300\text{ cm}^{-1}$ , in-plane vibrations of non-oxidized carbon C=C peaks at  $1500\text{--}1600\text{ cm}^{-1}$ , ketone group (C=O) at  $1600\text{--}1700\text{ cm}^{-1}$ , C=O vibrations from carboxyl (COOH) group at  $1740\text{--}1780\text{ cm}^{-1}$  and

hydroxyl (C–OH) at  $3400\text{--}3500\text{ cm}^{-1}$ . This is in line with the findings by XPS.

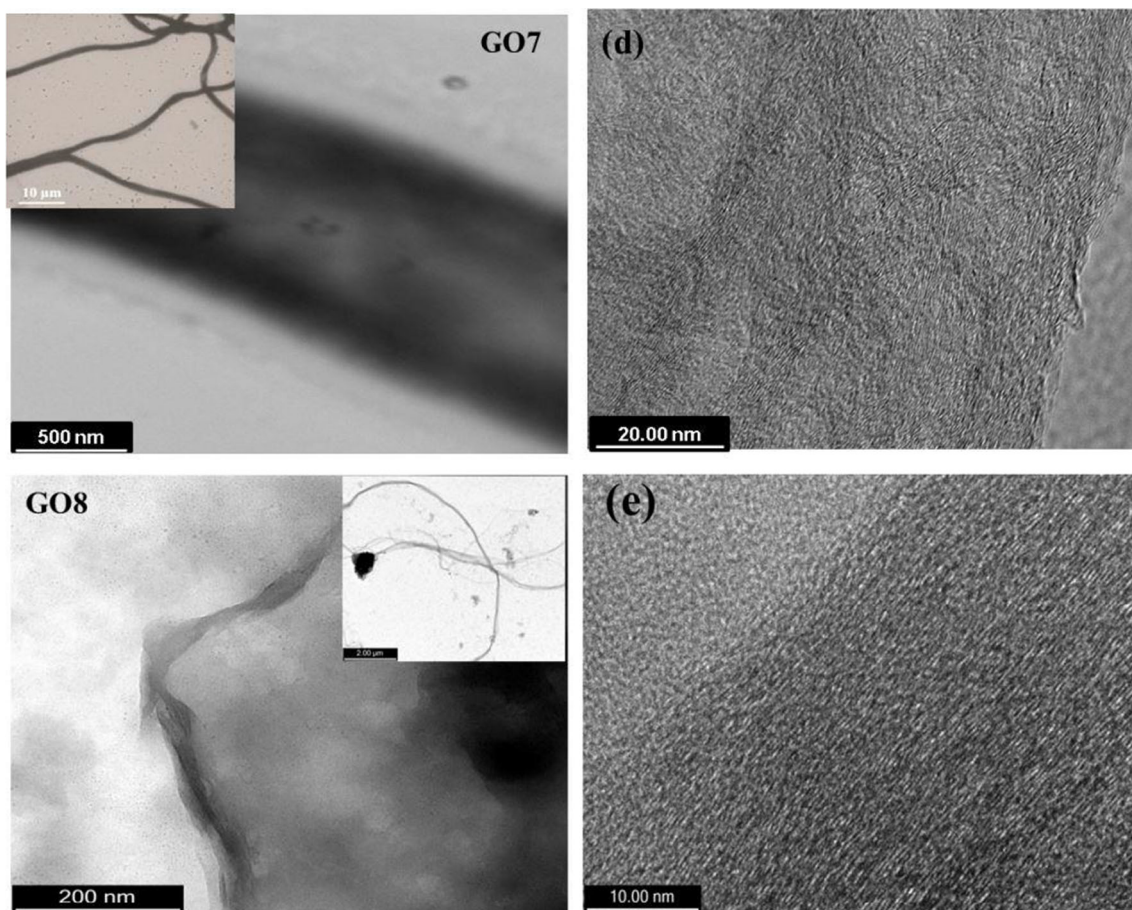


Figure 9 continued.

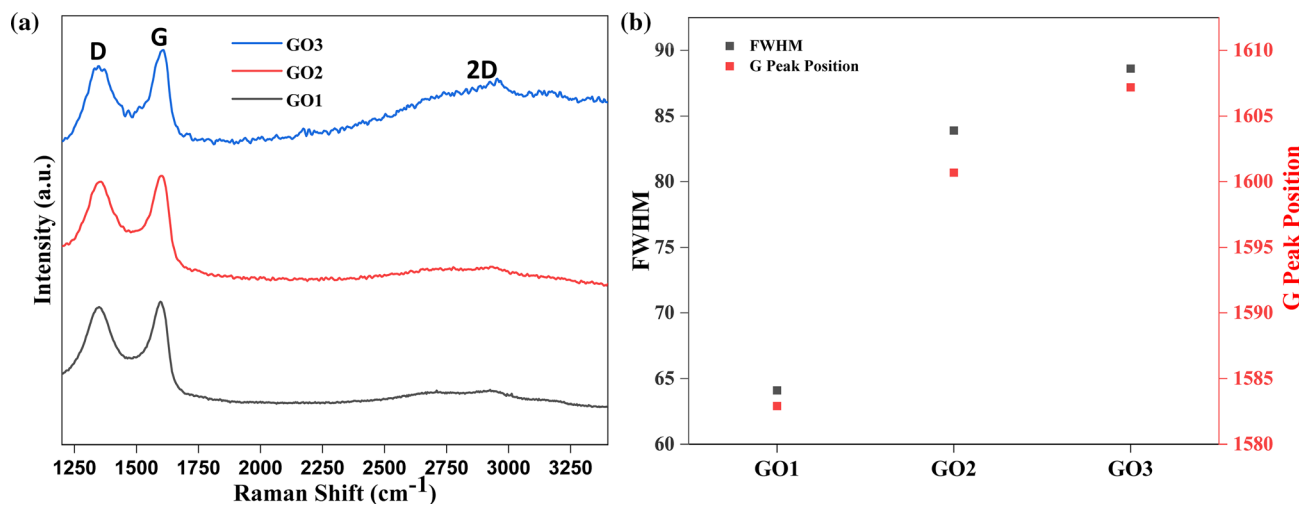
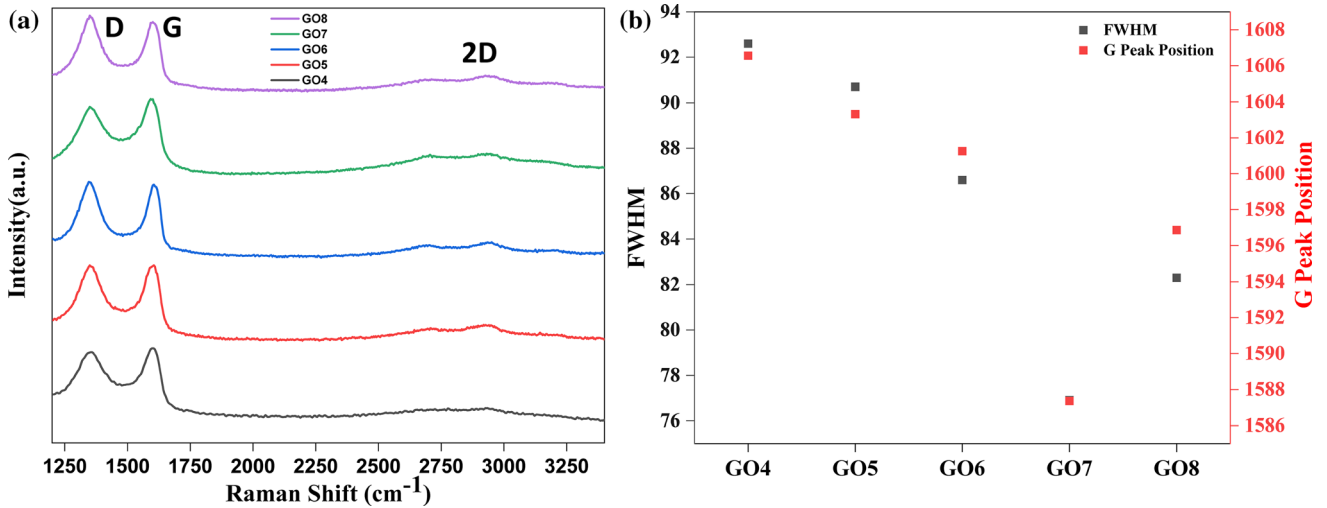
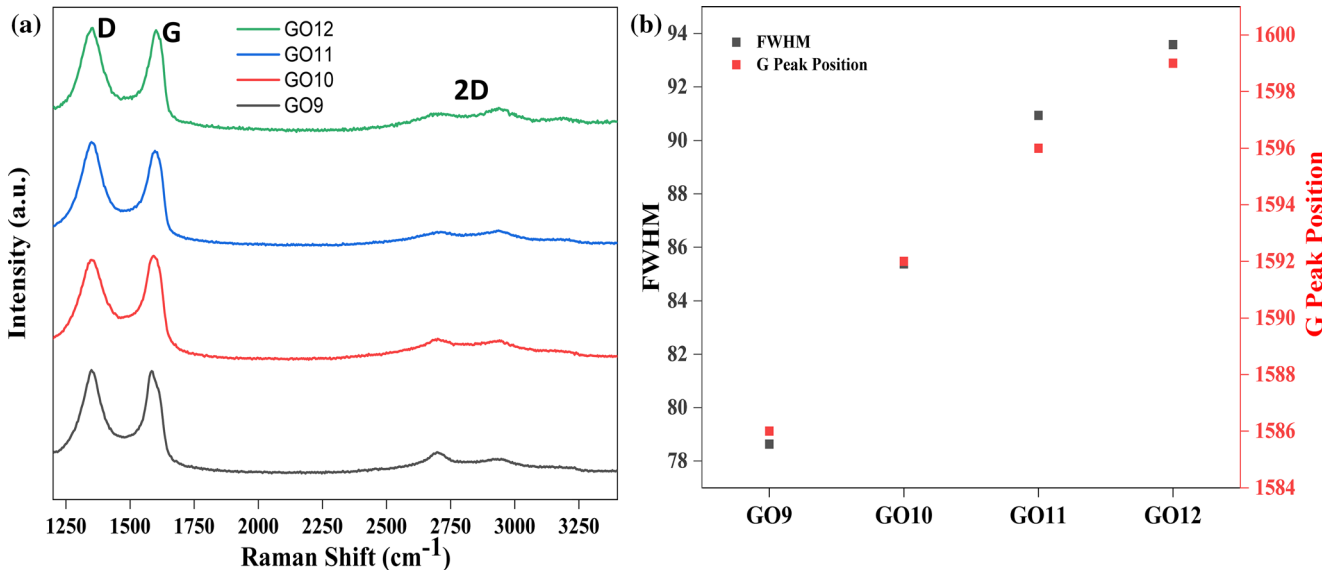


Figure 10 a Raman spectrum of graphene oxide samples GO1, GO2, GO3, stacked and b shift in peak position and FWHM of G peak is mapped for individual GO samples.



**Figure 11** a Raman spectra for samples GO4, GO5, GO6, GO7 and GO8 b shift in G peak position and FWHM is mapped for the above GO samples.



**Figure 12** a Raman spectra b shift in position and FWHM of G peak of samples GO9, GO10, GO11 and GO12.

### Discussion

Based on the experimental results and analyzed data, the following mechanism for the exfoliation mechanism is proposed. When the current is passed, the anions are transferred to the anode. During electrochemical exfoliation, the hydroxyl ions from electrolyte solution functionalizes the anodic graphite edges as well as at basal plane. This step helps in increasing the interlayer distance between the graphene sheets. Then the solvated sulfate ions intercalate into graphite layers and form an intermediate complex compound, i.e., graphite intercalated

compound. This complex compound then reacts with intercalated water molecule and form gases (O<sub>2</sub>, CO<sub>2</sub>, etc.). These gases then exert pressure on graphene layers and separate them out into thin layers. In our experiment, an aqueous solution of sulfuric acid has been used as the electrolyte at (1) varying and (2) constant pH conditions. In an aqueous system, the minimum potential to ionize the electrolyte is 1.2 V [66]. Since the applied bias was kept constant throughout the experiment at 6 V, intercalation and exfoliation were taking place in a single step. XPS analysis confirms the presence of different oxygen functional groups. For samples GO4 onwards NaOH

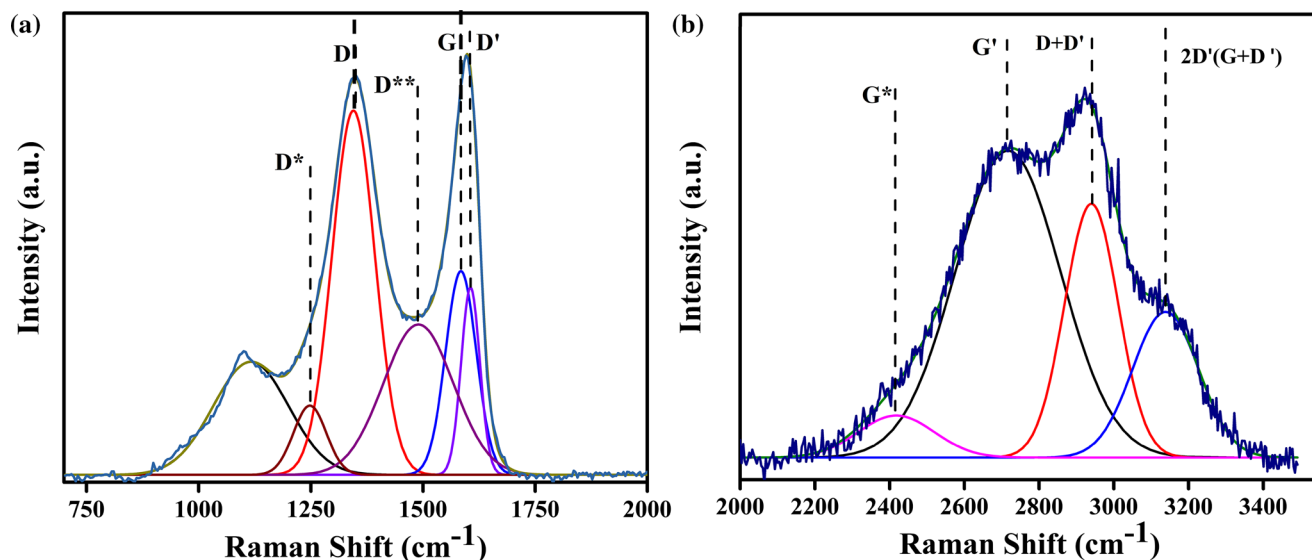


**Figure 13** Multiple peaks fitting for **a** G peak, D peak and **b** 2D peak.

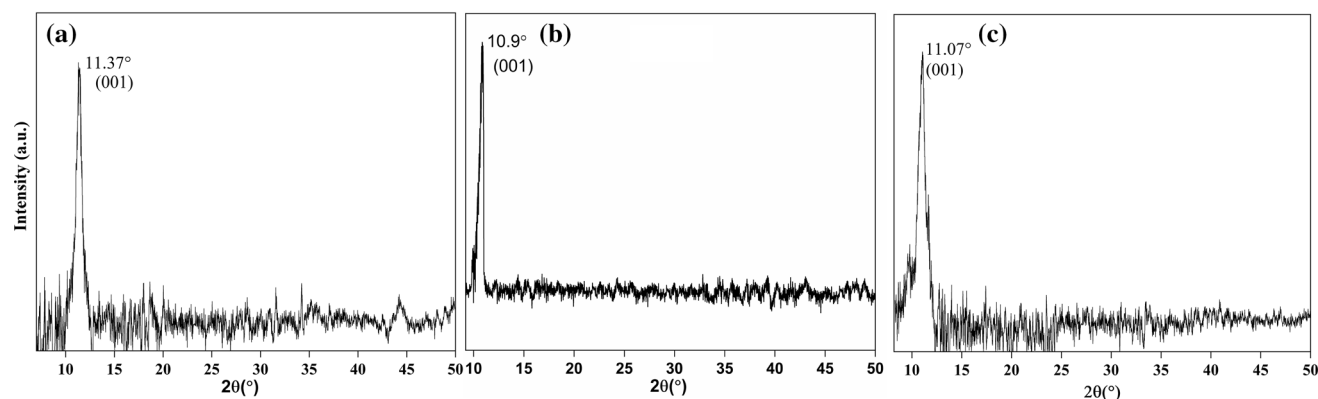


**Figure 14** XRD patterns for **a** GO1 **b** GO4 and **c** GO9.

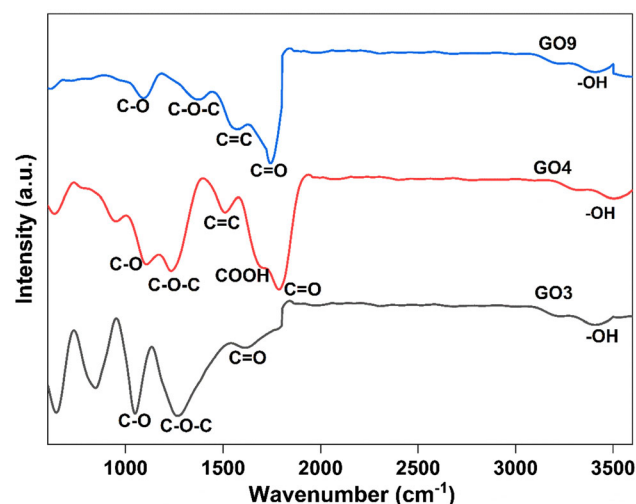


**Figure 15** FTIR spectrum of representative GO samples.

is added to the solution. The additional  $\text{OH}^-$  ions travel to the anode and attack the grain boundaries of graphite resulting in functionalization of them. This helps in easy exfoliation. On the other hand, the presence of  $\text{Na}^+$  ions in excess hinders the mobility of the sulfuric acid, thus reducing the exfoliation. Zhou et al. tried to explain the effect of resultant forces due to intercalated moieties on exfoliation pattern [67]. According to Tomcsanyi et al., it is seen that the adsorbed sulfate ions can be displaced in the presence of excess sulfate ions [68]. Therefore, two competitive processes occur simultaneously when NaOH is added. Depending on the pH of the solution, the dominance of one process prevails as explained in “Effect of electrolyte concentration” Section. Figure 16 indicates the regime map for the GO. Here the morphology of GO is mapped with respect to the



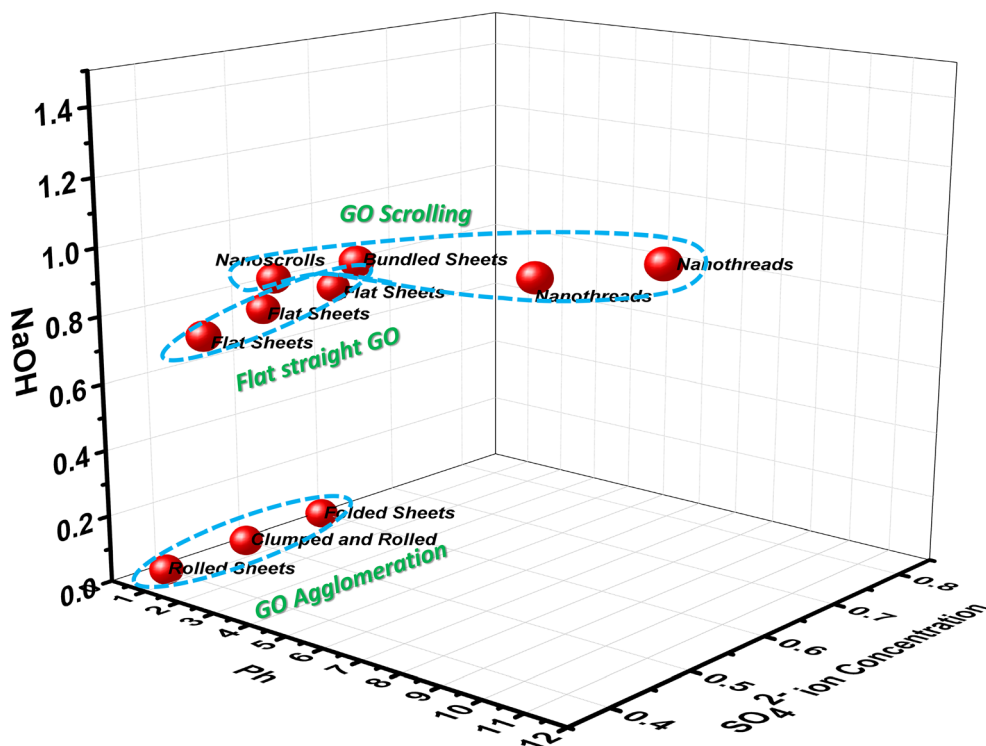


**Figure 16** Regime map for different geometries of GO observed at different pH conditions.

synthesis electrolyte composition. It helps in understanding the response of GO to the electrolyte dependent synthesis. It eases the understanding of the behavioral changes obtained with the alteration of the pH of the solution. This plot acts as a benchmark to develop an interesting GO morphological structure.

## Conclusions

The current research work shows a tunable strategy for GO synthesis by electrochemical exfoliation approach. The following conclusions can be drawn from our studies:

- (1) The geometry and the arrangement of graphite electrodes influenced the exfoliation and helped in the re-exfoliation of the graphite electrode.
- (2) For the first set of samples (GO1–GO3), where sulfuric acid concentration was increased by increasing the molarity of the solution, the GO exfoliation rate increased with the molarity.
- (3) In the second set of samples (GO4–GO8), the sulfuric acid concentration was kept constant at 0.5 M and the pH of the electrolyte was changed by the addition of NaOH. The addition of  $\text{OH}^-$  ions helps in exfoliation. On the other hand, the presence of  $\text{Na}^+$  ions, in excess, hinders the mobility of the sulfuric acid, thus reducing the exfoliation. GO4 showed the highest rate of exfoliation.
- (4) The third set of samples (GO9–GO12) was exfoliated at a constant pH of 2.5 with increasing molarity of sulfuric acid, where the maximum exfoliation rate was obtained 0.5 M.
- (5) XPS and FTIR analysis showed the presence of various functional groups on edges and basal planes of graphene depending on the exfoliation conditions.
- (6) TEM images revealed different morphologies of the sheet from flat sheet to folded sheet to nanoscroll to nanoribbon depending on the processing conditions.
- (7) In ethanol, the dispersion of GO samples showed stability more than 11 months irrespective of oxygen loading or synthesis condition.

## Acknowledgements

The authors would like to acknowledge Department of Atomic Energy, India, for providing a research fund.

**Supplementary Information:** The online version contains supplementary material available at <http://doi.org/10.1007/s10853-021-06535-4>.

## References

- [1] Low CTJ (2012) Electrochemical approaches to the production of graphene flakes and their potential applications. *Carbon N Y* 54:1–21. <https://doi.org/10.1016/j.carbon.2012.11.030>
- [2] Lavin-Lopez MP, Valverde JL, Sanchez-Silva L, Romero A (2016) Solvent-based exfoliation via sonication of graphitic materials for graphene manufacture. *Ind Eng Chem Res* 55(4):845–855. <https://doi.org/10.1021/acs.iecr.5b03502>
- [3] Go´mez-Navarro KKC, Thomas Weitz R, Bittner AM, Scolari M, Mews A, Burghard M (2007) Electronic transport properties of individual chemically reduced graphene oxide sheets. *Nano Lett.* 7(11):3499–503. <https://doi.org/10.1021/nl072090c>
- [4] Shin HJ et al (2009) Efficient reduction of graphite oxide by sodium borohydride and its effect on electrical conductance. *Adv Funct Mater* 19(12):1987–1992. <https://doi.org/10.1002/adfm.200900167>
- [5] Shao Y, Wang J, Engelhard M, Wang C, Lin Y (2010) Facile and controllable electrochemical reduction of graphene oxide and its applications. *J Mater Chem* 20(4):743–748. <https://doi.org/10.1039/b917975e>
- [6] Keeley GP, O’Neill A, McEvoy N, Peltekis N, Coleman JN, Duesberg GS (2010) Electrochemical ascorbic acid sensor based on DMF-exfoliated graphene. *J Mater Chem* 20(36):7864–7869. <https://doi.org/10.1039/c0jm01527j>
- [7] Robinson JT, Perkins FK, Snow ES, Wei Z, Sheehan PE (2008) Reduced graphene oxide molecular sensors. *Nano Lett* 8(10):3137–3140. <https://doi.org/10.1021/nl8013007>
- [8] Raccichini R, Varzi A, Passerini S, Scrosati B (2015) The role of graphene for electrochemical energy storage. *Nat Mater* 14(3):271–279. <https://doi.org/10.1038/nmat4170>
- [9] Solís-Fernández P, Bissett M, Ago H (2017) Synthesis, structure and applications of graphene-based 2D heterostructures. *Chem Soc Rev* 46(15):4572–4613. <https://doi.org/10.1039/c7cs00160f>
- [10] Wu Y et al (2010) Efficient and large-scale synthesis of few-layered graphene using an arc-discharge method and conductivity studies of the resulting films. *Nano Res* 3(9):661–669. <https://doi.org/10.1007/s12274-010-0027-3>
- [11] Edwards RS, Coleman KS (2013) Graphene synthesis: Relationship to applications. *Nanoscale* 5(1):38–51. <https://doi.org/10.1039/c2nr32629a>
- [12] Staudenmaier L (1898) Darstellung der graphitlure. *Ger Chem Soc* 31(2):1481–1487. <https://doi.org/10.1002/cber.18980310237>
- [13] G. Kationen and D. Beobachtung, “Hofmann Holst:Uber ” no. 28, pp. 754–771, 1939.
- [14] Hummers WS, Offeman RE (1958) Preparation of graphitic oxide. *J Am Chem Soc* 80(6):1339. <https://doi.org/10.1021/ja01539a017>
- [15] Li C, Shi Y, Chen X, He D, Shen L, Bao N (2018) Controlled synthesis of graphite oxide: formation process, oxidation kinetics, and optimized conditions. *Chem Eng Sci* 176:319–328. <https://doi.org/10.1016/j.ces.2017.10.028>
- [16] Zhong YL, Tian Z, Simon GP, Li D (2015) Scalable production of graphene via wet chemistry: progress and challenges. *Mater Today* 18(2):73–78. <https://doi.org/10.1016/j.mattod.2014.08.019>
- [17] Santamarı R, Granda M, Sierra U, Patricia A, Blanco C, Mene R (2014) A multi-step exfoliation approach to maintain the lateral size of graphene oxide sheets. *Carbon N Y* 80:830–832. <https://doi.org/10.1016/j.carbon.2014.08.053>
- [18] Chen J et al (2016) Synthesis of graphene oxide sheets with controlled sizes from sieved graphite flakes. *Carbon N Y* 110:34–40. <https://doi.org/10.1016/j.carbon.2016.08.096>
- [19] Esmaeili A, Entezari MH (2014) Facile and fast synthesis of graphene oxide nanosheets via bath ultrasonic irradiation. *J Colloid Interface Sci* 432:19–25. <https://doi.org/10.1016/j.jcis.2014.06.055>
- [20] Yuan R, Yuan J, Wu Y, Chen L, Zhou H, Chen J (2017) Efficient synthesis of graphene oxide and the mechanisms of oxidation and exfoliation. *Appl Surf Sci* 416:868–877. <https://doi.org/10.1016/j.apsusc.2017.04.181>
- [21] Asgar H, Deen KM, Riaz U, Ur Z, Hussain U, Haider W (2018) Synthesis of graphene via ultra-sonic exfoliation of graphite oxide and its electrochemical characterization. *Mater Chem Phys* 206:7–11. <https://doi.org/10.1016/j.matchemphys.2017.11.062>
- [22] Abulizi A, Okitsu K, Zhu J (2014) Ultrasound assisted reduction of graphene oxide to graphene in L-ascorbic acid aqueous solutions: Kinetics and effects of various factors on the rate of graphene formation. *Ultrason - Sonochem* 21(3):1174–1181. <https://doi.org/10.1016/j.ultsonch.2013.10.019>

- [23] Soltani T, Lee B (2017) Low intensity-ultrasonic irradiation for highly efficient, eco-friendly and fast synthesis of graphene oxide. *Ultrason - Sonochem* 38(2):693–703. <https://doi.org/10.1016/j.ultsonch.2016.08.010>
- [24] Botas C et al (2013) Optimization of the size and yield of graphene oxide sheets in the exfoliation step. *Carbon N Y* 63:576–578. <https://doi.org/10.1016/j.carbon.2013.06.096>
- [25] Qi X, Zhou T, Deng S, Zong G, Yao X, Fu Q (2014) Size-specified graphene oxide sheets: ultrasonication assisted preparation and characterization. *J Mater Sci* 49(4):1785–1793. <https://doi.org/10.1007/s10853-013-7866-8>
- [26] Li L et al (2020) Review—progress of research on the preparation of graphene oxide via electrochemical approaches. *J Electrochem Soc* 167(15):155519. <https://doi.org/10.1149/1945-7111/abbbc0>
- [27] Danial WH, Norhisham NA, Ahmad Noorden AF, Abdul Majid Z, Matsumura K, Iqbal A (2021) A short review on electrochemical exfoliation of graphene and graphene quantum dots. *Carbon Lett* 31(3):371–388. <https://doi.org/10.1007/s42823-020-00212-3>
- [28] Ljubek G, Čapeta D, Šrut Rakić I, Kraljić Roković M (2021) Energetically efficient and electrochemically tuneable exfoliation of graphite: process monitoring and product characterization. *J Mater Sci* 56(18):10859–10875. <https://doi.org/10.1007/s10853-021-05989-w>
- [29] Lu J, Yang J-X, Wang J, Lim A, Wang S, Loh KP (2018) One-pot synthesis of fluorescent carbon nanoribbons, nanoparticles, and graphene by the exfoliation of graphite in ionic liquids. *ACS Nano* 3(8):2367–2375. <https://doi.org/10.1021/nm900546b>
- [30] Chakrabarti MH et al (2015) One-pot electrochemical gram-scale synthesis of graphene using deep eutectic solvents and acetonitrile. *Chem Eng J* 274:213–223. <https://doi.org/10.1016/j.cej.2015.03.083>
- [31] Li L, Zhang D, Deng J, Fang J, Gou Y (2020) Review—preparation and application of graphene-based hybrid materials through electrochemical exfoliation. *J Electrochem Soc* 167(8):086511. <https://doi.org/10.1149/1945-7111/ab933b>
- [32] Liu N, Luo F, Wu H, Liu Y, Zhang C, Chen J (2008) One-step ionic-liquid-assisted electrochemical synthesis of ionic-liquid-functionalized graphene sheets directly from graphite. *Adv Funct Mater* 18(10):1518–1525. <https://doi.org/10.1002/adfm.200700797>
- [33] Parvez K et al (2014) Exfoliation of graphite into graphene in aqueous solutions of inorganic salts. *J Am Chem Soc* 136(16):6083–6091. <https://doi.org/10.1002/jcb.240530415>
- [34] Alanyalioglu M, Segura JJ, Oró-Sol J, Casañ-Pastor N (2012) The synthesis of graphene sheets with controlled thickness and order using surfactant-assisted electrochemical processes. *Carbon N Y* 50(1):142–152. <https://doi.org/10.1016/j.carbon.2011.07.064>
- [35] Danial WH, Chutia A, Majid ZA, Sahnoun R, Aziz M (2015) Electrochemical synthesis and characterization of stable colloidal suspension of graphene using two-electrode cell system. *AIP Conf Proc*, doi 10(1063/1):4919158
- [36] Yu P, Lowe SE, Simon GP, Zhong YL (2015) Electrochemical exfoliation of graphite and production of functional graphene. *Curr Opin Colloid Interface Sci* 20(5–6):329–338. <https://doi.org/10.1016/j.cocis.2015.10.007>
- [37] Li L, Zhang D, Gao Y, Deng J, Gou Y, Fang J (2021) Electric field driven exfoliation of MoS<sub>2</sub>. *J Alloys Compd*. <https://doi.org/10.1016/j.jallcom.2020.158551>
- [38] Li L, Zhang D, Deng J, Gou Y, Fang J (2020) Electrochemical exfoliation of two-dimensional layered black phosphorus and applications. *J Energy Chem* 49:365–374. <https://doi.org/10.1016/j.jechem.2020.03.010>
- [39] A. P. Johnson, H. V. Gangadharappa, and K. Pramod, *Graphene nanoribbons: A promising nanomaterial for biomedical applications*, vol. 325. Elsevier B.V, 2020.
- [40] Sontakke AD, Purkait MK (2021) A brief review on graphene oxide nanoscrolls: structure, synthesis, characterization and scope of applications. *Chem Eng J* 420(P1):129914. <https://doi.org/10.1016/j.cej.2021.129914>
- [41] Chen Z, Narita A, Müllen K (2020) Graphene nanoribbons: on-surface synthesis and integration into electronic devices. *Adv Mater* 32(45):1–26. <https://doi.org/10.1002/adma.202001893>
- [42] Fan Y et al (2010) A microexplosion method for the synthesis of graphene nanoribbons. *Carbon N Y* 49(4):1439–1445. <https://doi.org/10.1016/j.carbon.2010.12.013>
- [43] Mir A, Shukla A (2018) Electrochemical exfoliation of graphite to stage-III graphite bisulfate flakes in low concentration sulfuric acid solution: A novel synthesis route to completely trilayer graphene suspension. *Appl Surf Sci* 443:157–166. <https://doi.org/10.1016/j.apsusc.2018.02.284>
- [44] Chen J, Shi W, Xiong C (2018) Mixed solvent-mediated exfoliation of graphene invoked by synergistic effect of steric hindrance and hydrogen bond for improved electrochemical performance on its polymeric composites. *Electrochim Acta* 283:818–825. <https://doi.org/10.1016/j.electacta.2018.07.020>
- [45] Parvez K, Rincón RA, Weber N-E, Cha KC (2016) One-step electrochemical synthesis of nitrogen and sulfur co-doped, high-quality graphene oxide. *Chem Commun* 52:5714–5717. <https://doi.org/10.1039/C6CC01250G>
- [46] Zeng F, Kuang Y, Liu G, Liu R, Huang Z, Zhou H (2012) Nanoscale Supercapacitors based on high-quality graphene

- scrolls. *Nanoscale* 4:3997–4001. <https://doi.org/10.1039/c2nr30779k>
- [47] Zhao J et al (2014) Facile preparation of large-scale graphene nanoscrolls from graphene oxide sheets by cold quenching in liquid nitrogen. *Carbon* N Y. <https://doi.org/10.1016/j.carbon.2014.08.006>
- [48] Zhao J (2010) Efficient preparation of large-area graphene oxide sheets for transparent conductive films. *ACS Nano* 4(9):5245–5252
- [49] Ji E, Son J, Hun J, Lee G (2017) Rolling up two-dimensional sheets into nanoscrolls. *FlatChem*. <https://doi.org/10.1016/j.flatc.2017.09.002>
- [50] Stobinski L et al (2014) Graphene oxide and reduced graphene oxide studied by the XRD, TEM and electron spectroscopy methods. *J Electron Spectros Relat Phenomena* 195:145–154. <https://doi.org/10.1016/j.elspec.2014.07.003>
- [51] Wu H et al (2013) pH-dependent size, surface chemistry and electrochemical properties of graphene oxide. *Xinxing Tan Cailiao/New Carbon Mater* 28(5):327–335. [https://doi.org/10.1016/S1872-5805\(13\)60085-2](https://doi.org/10.1016/S1872-5805(13)60085-2)
- [52] Torrisi L et al (2018) Self-supporting graphene oxide films preparation and characterization methods. *Vacuum* 160:1–11. <https://doi.org/10.1016/j.vacuum.2018.11.001>
- [53] Torrisi L, Silipigni L, Cutroneo M (2018) Radiation effects of IR laser on graphene oxide irradiated in vacuum and in air. *Vacuum* 153:122–131. <https://doi.org/10.1016/j.vacuum.2018.04.010>
- [54] Libin Tang SPL, Li X, Ji R, Seng Teng K, Tai G, Ye J (2012) Bottom-up synthesis of large-scale graphene oxide nanosheets. *J. Mater. Chem.* 22:5676–5683. <https://doi.org/10.1039/c2jm15944a>
- [55] Lavin-Lopez MP, Paton-Carrero A, Sanchez-Silva L, Valverde JL, Romero A (2017) Influence of the reduction strategy in the synthesis of reduced graphene oxide. *Adv Powder Technol* 28(12):3195–3203. <https://doi.org/10.1016/j.apt.2017.09.032>
- [56] Sobon G et al (2012) Graphene oxide vs. reduced graphene oxide as saturable absorbers for er-doped passively mode-locked fiber laser. *Opt Expr* 20(17):19463–19473
- [57] Longo A et al (2017) Graphene oxide prepared by graphene nanoplatelets and reduced by laser treatment. *Nanotechnology* 28(2):224002
- [58] Perera D, Abeywickrama A, Zen F, Colavita PE, Jayasundara DR (2018) Evolution of oxygen functionalities in graphene oxide and its impact on structure and exfoliation: an oxidation time based study. *Mater Chem Phys* 220(May):417–425. <https://doi.org/10.1016/j.matchemphys.2018.08.072>
- [59] Kaniyoor A, Ramaprabhu S (2012) A raman spectroscopic investigation of graphite oxide derived graphene a raman spectroscopic investigation of graphite oxide derived graphene. *AIP Adv* 2(3):032183. <https://doi.org/10.1063/1.4756995>
- [60] De Silva KKH, Huang H, Yoshimura M (2018) A Progress of reduction of graphene oxide by ascorbic acid. *Appl Surf Sci* 447:338–346. <https://doi.org/10.1016/j.apsusc.2018.03.243>
- [61] LoDavid M, Mercedes VM (2017) Evolution of the Raman spectrum with the chemical composition of graphene oxide. *J Phys Chem C* 121(37):20489–20497. <https://doi.org/10.1021/acs.jpcc.7b06236>
- [62] Maria del Prado Lavin Lopez ARI, Valverde JL, Sanchez-Silva L (2016) Solvent-based exfoliation via sonication of graphitic materials for graphene manufacture. *Ind Eng Chem Res* 55(4):845–855. <https://doi.org/10.1021/acs.iecr.5b03502>
- [63] Childres I, Jauregui LA, Park W, Cao H, Chen YP (2013) Raman Spectroscopy of graphene and related materials. *New Dev Phot Mater Res* 1:1–20
- [64] King AAK et al (2016) A new Raman metric for the characterisation of graphene oxide and its derivatives. *Nat Publ Gr*. <https://doi.org/10.1038/srep19491>
- [65] Li H et al (2018) Superior adhesion of graphene nanoscrolls. *Commun Phys* 1(1):1–7. <https://doi.org/10.1038/s42005-018-0043-2>
- [66] Li Le et al (2020) Electrochemical synthesis of 2D antimony, bismuth and their compounds. *J Mater Chem C* 8(28):9464–9475
- [67] Zhou M, Tang J, Cheng Q, Xu G, Cui P, Qin LC (2013) Few-layer graphene obtained by electrochemical exfoliation of graphite cathode. *Chem Phys Lett* 572:61–65. <https://doi.org/10.1016/j.cplett.2013.04.013>
- [68] Tomcsanyi K, Varga L, Horanyi G (1989) Electrochemical study of the pitting corrosion of aluminium and its alloys-ii. study of the interaction of chloride ions with, a passive film on aluminium and initiation of pitting corrosion. *Electrochim Acta* 34(6):855–859

**Publisher's Note** Springer Nature remains neutral with regard to jurisdictional claims in published maps and institutional affiliations.